



Identification of the extracellular matrix protein Fibulin-2 as a regulator of spinal nerve organization



Julia Schaeffer^{a,*}, David Tannahill^b, Jean-Michel Cioni^a, Dáire Rowlands^c, Roger Keynes^a

^a Department of Physiology, Development and Neuroscience, University of Cambridge, UK

^b Cancer Research UK Cambridge Institute, UK

^c Cambridge John van Geest Centre for Brain Repair, UK

ARTICLE INFO

Keywords:

RNA-sequencing

Chick

Sclerotome

Spinal nerve

Extracellular matrix

Fibulin-2

ABSTRACT

During amniote peripheral nervous system development, segmentation ensures the correct patterning of the spinal nerves relative to the vertebral column. Along the antero-posterior (rosto-caudal) axis, each somite-derived posterior half-sclerotome expresses repellent molecules to restrict axon growth and neural crest migration to the permissive anterior half-segment. To identify novel regulators of spinal nerve patterning, we investigated the differential gene expression of anterior and posterior half-sclerotomes in the chick embryo by RNA-sequencing. Several genes encoding extracellular matrix proteins were found to be enriched in either anterior (e.g. Tenascin-C, Laminin alpha 4) or posterior (e.g. Fibulin-2, Fibromodulin, Collagen VI alpha 2) half-sclerotomes. Among them, the extracellular matrix protein Fibulin-2 was found specifically restricted to the posterior half-sclerotome. By using *in ovo* ectopic expression in chick somites, we found that Fibulin-2 modulates spinal axon growth trajectories *in vivo*. While no intrinsic axon repellent activity of Fibulin-2 was found, we showed that it enhances the growth cone repulsive activity of Semaphorin 3A *in vitro*. Some molecules regulating axon growth during development are found to be upregulated in the adult central nervous system (CNS) following traumatic injury. Here, we found increased Fibulin-2 protein levels in reactive astrocytes at the lesion site of a mouse model of CNS injury. Together, these results suggest that the developing vertebral column and the adult CNS share molecular features that control axon growth and plasticity, which may open up the possibility for the identification of novel therapeutic targets for brain and spinal cord injury.

1. Introduction

The process of segmentation is fundamental in the organization of the vertebrate trunk. It can be observed early during development with the sequential formation of transient, multipotent structures, the mesodermal somites. Somites differentiate subsequently into dermatome (dermis precursor), myotome (muscle precursor) and sclerotome (cartilage and bone precursor), in response to signaling of synergistic molecules such as Shh-induced transcription factors, BMP antagonists and members of the Wnt family (reviewed in (Scaal, 2016)). The sclerotome itself undergoes internal regionalization events (mediolateral, dorso-ventral and antero-posterior) that are essential to the formation of various elements of the vertebral column and to the development of the peripheral nervous system (Fleming et al., 2015).

In amniotes, the polarization of the sclerotome along the antero-posterior axis is key for the development of the peripheral nervous system (PNS). Each sclerotome subdivides into two halves (anterior, A, and posterior, P) with an intrasegmental boundary that is morphologi-

cally visible from somite V (5th most recent segment (Christ and Ordahl, 1995)). The development of spinal nerves is governed by the intrinsic molecular differences between the anterior and the posterior half-sclerotomes, which allow optimal integration of the emerging spinal nerves in the vertebral column (Keynes and Stern, 1984; Bronner-Fraser and Stern, 1991). The anterior half-sclerotome is permissive for the migration of neural crest cells and for the outgrowth of motor axons (Fig. 1A). Neural crest-derived dorsal root ganglia (DRG) form in the anterior half, and sensory axons are also confined in the anterior half when projecting to the neural tube. The posterior half-sclerotome, on the other hand, possesses repulsive properties that play an essential role in this segmentation process. Several repellent molecules, such as members of the Semaphorin family and Ephrins, are expressed in the posterior half-sclerotome and are responsible, at least in part, for the segmented pattern of neural crest cell migration and motor axon outgrowth (Kuan et al., 2004; Bonanomi and Pfaff, 2010). Some evidence for their repulsive role has been provided *in vivo*, but each candidate molecule does not account by itself for the segmentation process undergone by

* Corresponding author.

E-mail address: julia.schaeffer13@gmail.com (J. Schaeffer).

<https://doi.org/10.1016/j.ydbio.2018.06.014>

Received 27 September 2017; Received in revised form 24 May 2018; Accepted 19 June 2018

Available online 23 June 2018

0012-1606/ © 2018 The Authors. Published by Elsevier Inc. This is an open access article under the CC BY-NC-ND license (<http://creativecommons.org/licenses/by-nc-nd/4.0/>).

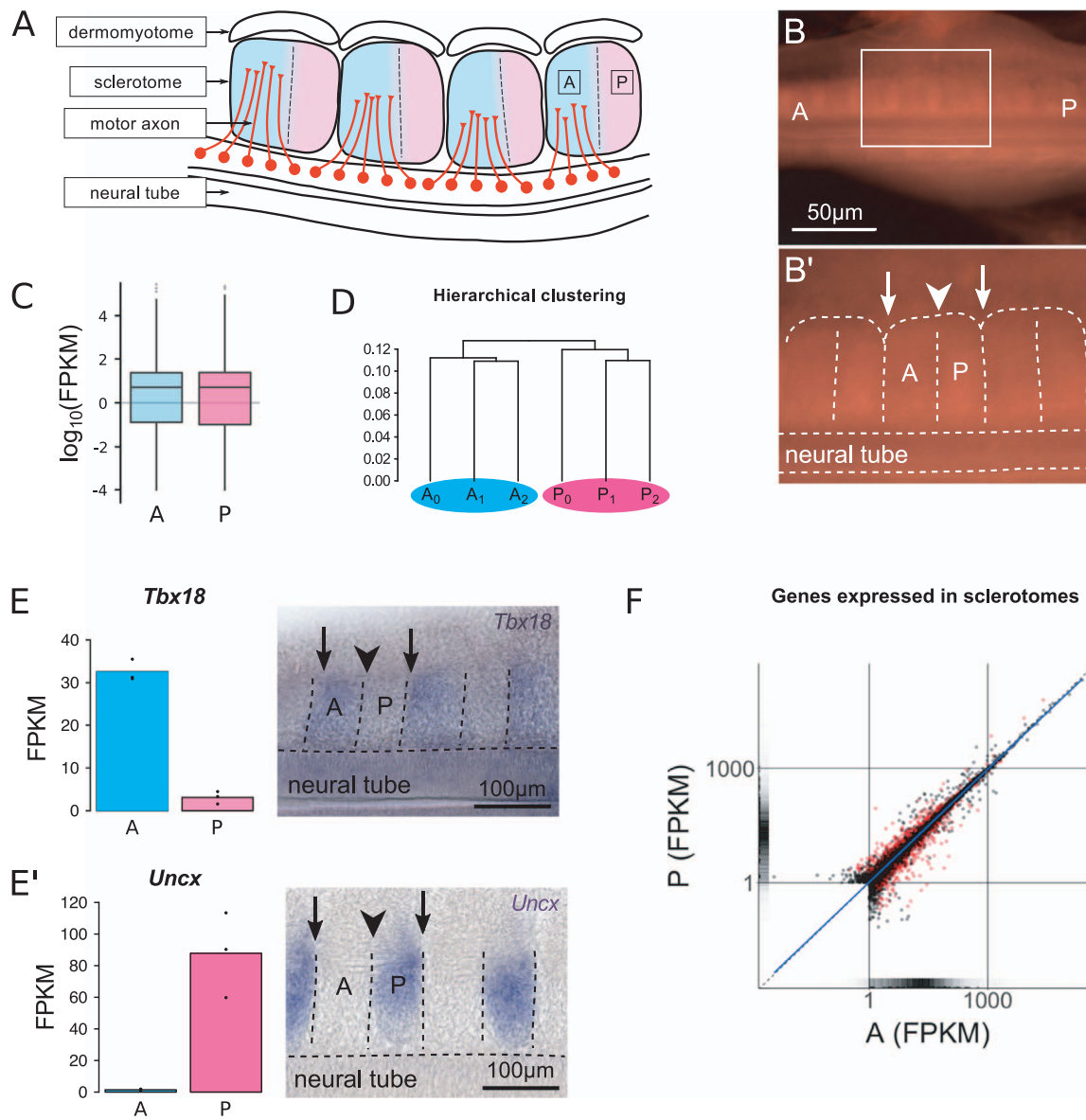


Fig. 1. Differential gene expression analysis between anterior and posterior half-sclerotomes. (A) Schematic representation of motor axon segmental outgrowth governed by the intrinsic differences between anterior (A) and posterior (P) half-sclerotomes. (B) Picture of a live chick embryo of embryonic day 3 (stage HH18). The segmented pattern of mesodermal somites is visible on each side of the neural tube. A: anterior end of the embryo. P: posterior end. (B') Zoom of picture (B). The arrows indicate the intersomitic boundaries between adjacent segments. The arrowhead indicates the intrasegmental boundary (von Ebner's fissure) between anterior (A) and posterior (P) half-sclerotomes. (C) Boxplots representing the distribution of Fragments Per Kilobase of transcript per Million mapped reads (FPKM) for A and P sample groups. (D) Dendrogram representing hierarchical clustering of sample replicates for RNA-sequencing. (E-E') Barplots representing FPKM values for *Tbx18* and for *Uncx*. *In situ* hybridization for *Tbx18* and *Uncx* showing their preferential expression in the anterior (A) and the posterior (P) half-sclerotome, respectively. The arrows indicate the intersomitic boundaries between adjacent segments. The arrowhead indicates the intrasegmental boundary. (F) Scatterplot comparing FPKM values in anterior (A) and posterior (P) sample groups for 11113 genes expressed in sclerotomes (FPKM ≥ 1 in A or P sample groups). Genes that are significantly differentially expressed are represented with red dots. Plots (C) and (D) were generated with CummeRbund R package.

spinal nerves, unless accompanied with somite polarity defects (Lewcock et al., 2007; Bai et al., 2011). For example, *Nrp1*^{Sema-} knockin mice (where specific binding of Neuropilin-1 (Nrp1) to Semaphorin 3A (Sema3A) is selectively abolished) and Neuropilin-2 (Nrp2)-knockout mice exhibit large defasciculation in spinal motor projections, and these defects are enhanced in *Nrp1*^{Sema-};*Nrp2*^{-/-} double mutants (Huber et al., 2005). In the posterior half-sclerotome, Semaphorin 3F (Sema3F) restricts the initial outgrowth of motor axons to the anterior half-sclerotome, while Sema3A promotes fasciculation of ventral roots (Roffers-Agarwal and Gammill, 2009). However, the initial segmentation of motor axons when outgrowing of the neural tube is preserved in the *Nrp* double mutants (Huber et al., 2005), suggesting the existence of an additional molecular mechanism that specifies the antero-posterior trajectory within each segment.

Here we took advantage of high-throughput sequencing to give an up-to-date molecular map of anterior and posterior half-sclerotomes, using the chick embryo as a model organism. We identified molecules differentially expressed in half-sclerotomes and previously uncharacterized in this system, with a particular enrichment of genes encoding extracellular matrix (ECM) proteins, membrane proteins and proteins associated with ECM structures. One protein of the ECM, Fibulin-2, was found specifically restricted to the posterior half-sclerotome. Fibulin-2 belongs to a family of conserved ECM and ECM-associated proteins that act as matrix organizers in various organs (Vega et al., 2009). We observed that Fibulin-2 segmented pattern of expression coincides with the initial segmentation of spinal nerves along the antero-posterior axis. In addition, ectopic overexpression of Fibulin-2 in both halves of the sclerotome leads to a spatial restriction of spinal

nerve growth along the antero-posterior axis. Although Fibulin-2 does not have an intrinsic repulsive activity, our *in vitro* data suggest that Fibulin-2 enhances the biological activity of the axon growth repellent Sema3A to cause growth cone collapse. It is thought that molecular pathways involved in the regulation of axon guidance in the developing embryo are reactivated during nerve injury in the adult. Therefore we looked at this newly identified gene in the context of axon regeneration and we found that Fibulin-2 is specifically expressed by reactive astrocytes at the lesion site following brain injury in the adult central nervous system (CNS), suggesting that Fibulin-2-associated function in axon growth modulation is present in the adult nervous system. Together, these results illustrate the idea that some developmental mechanisms of axon patterning are reactivated in the adult CNS following traumatic injury, and their understanding may have significant implications for CNS repair strategies.

2. Results

2.1. RNA-sequencing on microdissected anterior and posterior half-sclerotomes reveals an enrichment of extracellular matrix proteins

Anterior (A) and posterior (P) half-sclerotomes were microdissected from chick embryos of stage Hamburger Hamilton (HH) 18 (Hamburger and Hamilton, 1951) (embryonic day 3) from somite XI to somite XXIII (11th to 23rd most recent segments (Christ and Ordahl, 1995)). At this stage the subdivision of the sclerotome into two halves – anterior and posterior – is morphologically visible (Fig. 1B), which enables an enrichment of each pool with minimal cross-contamination. We focused on the differences between two distinct populations, rather than on the mechanisms that establish the polarization in earlier somites.

RNA-sequencing was performed on three pools of 100 half-sclerotomes of each half (anterior, A, and posterior, P). The percentage of uniquely mapped reads was > 89% for each sample (Supplementary material Table 1). The distribution of Fragments Per Kilobase of transcript per Million mapped reads (FPKM) is shown on Fig. 1C and is similar in both sample groups. To rule out false-positive results, genes with a low expression level (FPKM < 1 in both A and P) were filtered out, resulting in a gene set containing 11113 genes (65% of total number of genes). A dendrogram of this gene set based on Jensen-Shannon distance allowed visualization of the relationship between biological replicates and confirmed that A and P samples cluster together (Fig. 1D). To control for the quality of microdissection and sample preparation, we looked at the expression values for control genes that were previously determined to be differentially expressed between the two half-sclerotomes. *Tbx18* (a marker for anterior half-sclerotome (Kraus et al., 2001)) was largely represented in A samples (average FPKM: 32.54) with very low detection in P samples (average FPKM: 3.10) (Fig. 1E). *Uncx* (a marker for posterior half-sclerotome (Mansouri et al., 1997)) was largely represented in P samples (average FPKM: 87.84) with very low detection in A samples (average FPKM: 1.45) (Fig. 1E'). These data confirmed the accuracy of the microdissection and provided a control for the rest of the analysis and for the identification of novel differentially expressed genes.

Using the program Cuffdiff, we found 744 genes differentially expressed (P -value < 0.05 with a false discovery rate (FDR) correction of 0.05), including 309 with a \log_2 fold change > 1 (Fig. 1F and Supplementary material Table 2). As both halves will later contribute to the vertebra (through a process of resegmentation), it was not surprising to find a relatively small molecular difference between them.

Functional annotation of the 744 differentially expressed genes revealed specific functional clusters enriched in anterior or in posterior half-sclerotomes. We visualized the functional annotation with the Cytoscape plug-in Enrichment Map (Fig. 2A) and we identified extracellular matrix (ECM) proteins and ECM-associated processes as one of the most enriched clusters in both anterior and posterior half-

sclerotomes (DAVID enrichment score: 7.72). Sample group A showed a functional enrichment in cell adhesion and focal adhesion, while sample group P showed a functional enrichment of functional domains such as immunoglobulin domain and EGF-like calcium-binding domain.

The functional classification with annotations of the cellular component (CC) gene ontology revealed that each half is enriched with proteins of the extracellular matrix (proteinaceous extracellular matrix, fold enrichment = 3.72, P -value = 9.14×10^{-9}) (Fig. 2B). Genes encoding proteins of the ECM, but also involved in ECM remodeling and processing were found. Other functional categories include cell surface components (fold enrichment = 2.51, P -value = 2.45×10^{-6}) and specific extracellular structures, such as focal adhesion (fold enrichment = 2.21, P -value = 6.02×10^{-5}) and basement membrane (fold enrichment = 4.70, P -value = 7.70×10^{-5}). The anterior half-sclerotome expresses genes associated with integrin complexes (fold enrichment = 8.27, P -value = 4.66×10^{-4}). The enriched expression of collagen trimers (fold enrichment = 5.27, P -value = 7.22×10^{-5}) in both the anterior and the posterior half is also consistent with the fact that the sclerotome will later undergo chondrogenesis and differentiate into cartilage. ECM molecules found among genes differentially expressed (FDR-corrected P -value < 0.05 and \log_2 fold change > 1) include Periostin, Tenascin-C and Laminin alpha 4 in anterior half-sclerotomes, and Fibulin-2, Fibromodulin and Collagen VI alpha 2 in posterior half-sclerotomes (Fig. 2C).

2.2. Identification of novel genes preferentially expressed in anterior or posterior half-sclerotomes

Chick embryos of embryonic day 3 (stage HH18) were used to validate gene expression by whole-mount *in situ* hybridization (Fig. 3 and Supplementary material Fig. 1). The ECM molecules Fibulin-2, Collagen VI alpha 2 and Fibromodulin were confirmed to be enriched in the posterior half-sclerotome (Fig. 3A–C), while the extracellular matrix glycoprotein Tenascin-C was confirmed to be expressed in the anterior half-sclerotome (Supplementary material Fig. 1E), where it is produced by neural crest cells at early stages of migration (Tucker, 2001). Interestingly, some genes show a variable level of expression along the antero-posterior axis. For example, Fibromodulin preferential expression in the posterior half-sclerotome disappears in more mature somites (Fig. 3C). The cell surface receptor Contactin-2 and the cell adhesion molecule Cadherin-7 are expressed in the anterior half-sclerotome, possibly by neural crest cells to support their migration in this half (Fig. 3D and F). The anterior half-sclerotome also expresses genes associated with retinoic acid signaling (e.g. *Crabp1*, *Rxrg*) (Fig. 3E and Supplementary material Fig. 1F), consistent with a role in neurite outgrowth and axonal elongation (Clagett-Dame et al., 2006). Among the repulsive guidance cues previously identified in this system, Ephrin-B1 and Sema3F, a member of the Semaphorin family with axon growth repulsion activity, were confirmed to be expressed in the posterior half-sclerotome only (Supplementary material Fig. 1A and C). Cadherin-13, a non-classical member of the cadherin superfamily shown to possess axon growth repulsive activity (Fredette et al., 1996), was found enriched in the posterior half-sclerotome (Supplementary material Fig. 1D). The axon growth repellent Sema3A was also found to be preferentially expressed in the posterior half-sclerotome (fold change P versus A: 1.38, FDR-corrected P -value: 0.0190) (Supplementary material Fig. 1B), consistent with previous descriptions of its expression. This small fold change in Sema3A expression between posterior and anterior half-sclerotomes is most likely due to the range of somite stages that we dissected for this molecular characterization by RNA-sequencing (somite XI to somite XXIII). Indeed, Sema3A preferential expression in the posterior half-sclerotome is not set at early somite stages (not before stage HH15 in chick (Eickholt et al., 1999) and stage E10.0 in mouse (Roffers-Agarwal and Gammill, 2009)). Second, Sema3A has been shown to be expressed

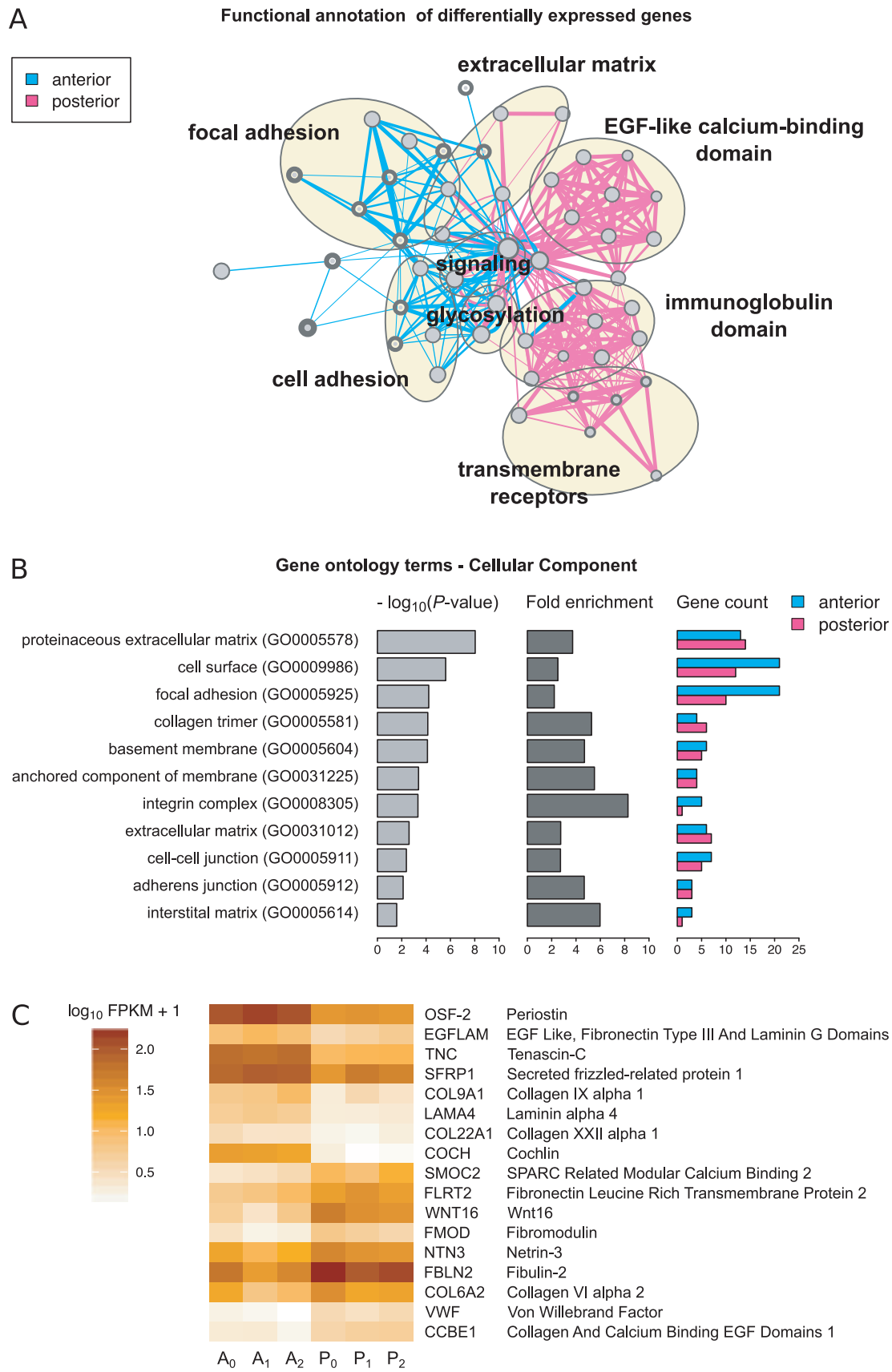


Fig. 2. Functional annotation of differentially expressed genes. (A) Enrichment map for genes differentially expressed in anterior or posterior half-sclerotomes. Each node represents a pathway or a gene ontology term. Links between nodes represent the genes shared by both pathways (P -value cutoff: 0.001, FDR Q -value cutoff: 0.05, overlap coefficient: 0.6). The map was generated with the Cytoscape plug-in Enrichment Map. Clusters were manually drawn and annotated. Nodes not connected to the main network are not represented. (B) Functional annotation in Cellular Component gene ontology terms of differentially expressed genes using DAVID bioinformatics database. Selection of terms in the top 21 gene ontology terms for Cellular Component. The P -value is the modified Fisher Exact P -value (EASE score) for gene enrichment analysis, as calculated by DAVID. A P -value < 0.05 ($-\log_{10}(P\text{-value}) > 1.3$) indicates a strong enrichment of a functional annotation category. For each gene ontology term, the fold enrichment and the number of genes expressed in each half-sclerotome are indicated. (C) Heatmap representing FPKM values for genes differentially expressed in anterior or posterior half-sclerotomes (FDR-corrected P -value < 0.05 and \log_2 fold change > 1) and functionally annotated as extracellular matrix in Cellular Component gene ontology terms. Heatmap generated with CummeRbund R package.

intrinsically by spinal motor neurons and to regulate their response to environmental (extrinsic) *Sema3A* during peripheral innervation (Moret et al., 2007), so this might explain why *Sema3A* is detected in the anterior half-sclerotome.

2.3. *Fibulin-2* is expressed in posterior half-sclerotomes and contributes to spinal nerve bundle shaping

We focused on one gene expressed in the posterior half-sclerotome, the ECM glycoprotein *Fibulin-2*. *Fibulin-2* is among the top 50 genes expressed in the posterior half-sclerotome with a \log_2 fold change > 1 (fold change P versus A : 3.59; Fig. 3A). Interestingly, we found that the segmented pattern of expression of *Fibulin-2* coincides temporally with the initial segmentation of outgrowing motor axons. *Fibulin-2* is preferentially expressed in the posterior half-sclerotome from somite stage XII, as observed with whole-mount *in situ* hybridization on stage HH14 embryos (embryonic day 2.5, E2.5) (Fig. 4A). The segmented projection of spinal nerves out of the neural tube was observed from somite stage XIII with *Tubulin 3 β* (TUJ1) immunostaining on embryos of the same stage (Fig. 4B). Some axon growth repellents known to contribute to spinal nerve segmentation do not show a similar temporal regulation. For example *Sema3A* preferential expression in the posterior half-sclerotome is not set before stage HH15 in chick (Eickholt et al., 1999) and our own observations, data not shown). Therefore we decided to test functionally the role of *Fibulin-2* in spinal nerve organization.

We validated *Fibulin-2* expression in posterior half-sclerotomes at the protein level using a polyclonal anti-*Fibulin-2* antibody directed against a region of the protein that is conserved between chick and human. *Fibulin-2* expression is complementary to nerve bundles forming in the anterior half-sclerotome (Fig. 4C and D). *Fibulin-2* expression in the posterior half-sclerotome persists through to at least embryonic day 4 (stage HH22) (Fig. 4E and F).

In addition, *Fibulin-2* is strongly expressed in the perinotochordal region, as observed on transverse sections of E2.5 chick embryos (Supplementary material Fig. 2A). The protein is most likely secreted by the notochord itself, as the notochord was observed to express *Fibulin-2* in whole-mount *in situ* hybridization on E2.5 chick embryos (Supplementary material Fig. 2B). The notochord secretes axon growth repulsive cues and participates in the organization of DRG axon projections along the dorso-ventral axis during development (Keynes et al., 1997). In addition, the notochord participates in the formation of the vertebrae by producing bone matrix, suggesting a possible role for *Fibulin-2* in chondrogenesis and/or cartilage formation during development of the vertebral column.

In order to investigate the role of *Fibulin-2* in the posterior half-sclerotome, a local overexpression approach was taken, based on somite electroporation. The experimental strategy was to overexpress *Fibulin-2* in both anterior and posterior half-sclerotomes. The principle of somite electroporation, as described in (Wang et al., 2011), requires to microinject of the construct in somites at the epithelial stage, and to target the medio-ventral region corresponding to the presumptive sclerotome (Fig. 5A). For this approach, we used an expression vector based on the viral T2A peptide system (Bourgeois et al., 2015), which enables the expression of two proteins (gene of interest and reporter) in stoichiometric proportions. We electroporated chick embryos of stage HH13–14 and we consistently targeted somite III (third most recent

segment) to somite VIII. The ectopic expression of the reporter was observed 24 h post-electroporation, when embryos reached stage HH18, at which point analysis was performed (Fig. 5B).

Fibulin-2 local overexpression 24 h post-electroporation was confirmed with immunohistochemistry on sections (Supplementary material Fig. 3). We analyzed the effects on spinal nerve outgrowth by whole-mount immunohistochemistry for the neuronal marker *Tubulin 3 β* (TUJ1). In control embryos, spinal axons grow in the anterior half-sclerotome, using all the available space between the repulsive posterior half-sclerotomes (Fig. 5C). In experimental embryos (*Fbln2*), spinal axons are still segmented when growing towards the periphery, but their growth in GFP-positive segments is more confined (Fig. 5D), a phenotype also observed in hypomorphic *Supt20* mutant mouse embryos (Warrier et al., 2017). The width of the bundles along the antero-posterior axis is restricted, suggesting that the ectopic expression of *Fibulin-2* further confines axon growth within each segment. This observation was quantified by measuring the area of each bundle from its most medial point (adjacent to the neural tube) to its most lateral point. For each segment, the nerve bundle area gives a measure of how confined the bundles are in GFP-positive segments (Fig. 5F). Only embryos of the same stage (HH18) and that did not show important electroporation-related morphological defects were kept for the analysis. Segments were measured at the same axial level. We measured 52 segments over 10 control embryos and 38 segments over 7 *Fbln2*-electroporated embryos. The nerve bundle area was significantly different in *Fbln2*-electroporated embryos compared to control embryos (26.7% decrease, t -test, P -value = $7.96e-04$) (Fig. 5G). By way of comparison and in order to confirm our experimental approach, we electroporated chick *Sema3A* cloned in the T2A vector and found a strong effect on axon confinement due to its repulsive activity (Fig. 5E) with a significant drop in the nerve bundle area (54.5% decrease, t -test, P -value = $3.03e-07$) (Fig. 5G).

To determine whether the ectopic misexpression of *Fibulin-2* induces defects in somite polarity, we used *in situ* hybridization to look at the expression of *Uncx*, a marker of the posterior half-sclerotome. No defect was observed when comparing control and experimental embryos (Supplementary material Fig. 4), implying that the confinement of spinal nerves is not due to a modification of sclerotome polarity induced by the local overexpression. Moreover, we did not detect any expression of *Caspase-3* by immunostaining (data not shown), suggesting that the decrease in nerve bundle area is not due to increased neuronal cell death.

2.4. *Fibulin-2* enhances *Sema3A* axon growth repulsive activity

To elucidate the mechanism of *Fibulin-2*-induced confinement of spinal nerves, we used the *in vitro* growth cone collapse assay. Recombinant human *Fibulin-2* was tested at various concentrations for its repulsive potential and did not show any significant effect at 100 ng/ml (19.7% collapsed growth cones) and 500 ng/ml (20.8%), compared to PBS (16.6%) (t -tests, P -value = 0.102 and 0.114, respectively). Even at a high concentration (1 μ g/ml), *Fibulin-2* did not show any marked collapse activity after 30 min of treatment (21.6%) (t -test, P -value = 0.0331) (Fig. 6A).

As a key ECM organizer, we hypothesized that *Fibulin-2* associates with a repellent molecule expressed in the posterior half-sclerotome to repel axon growth. This was tested with the potent axon growth

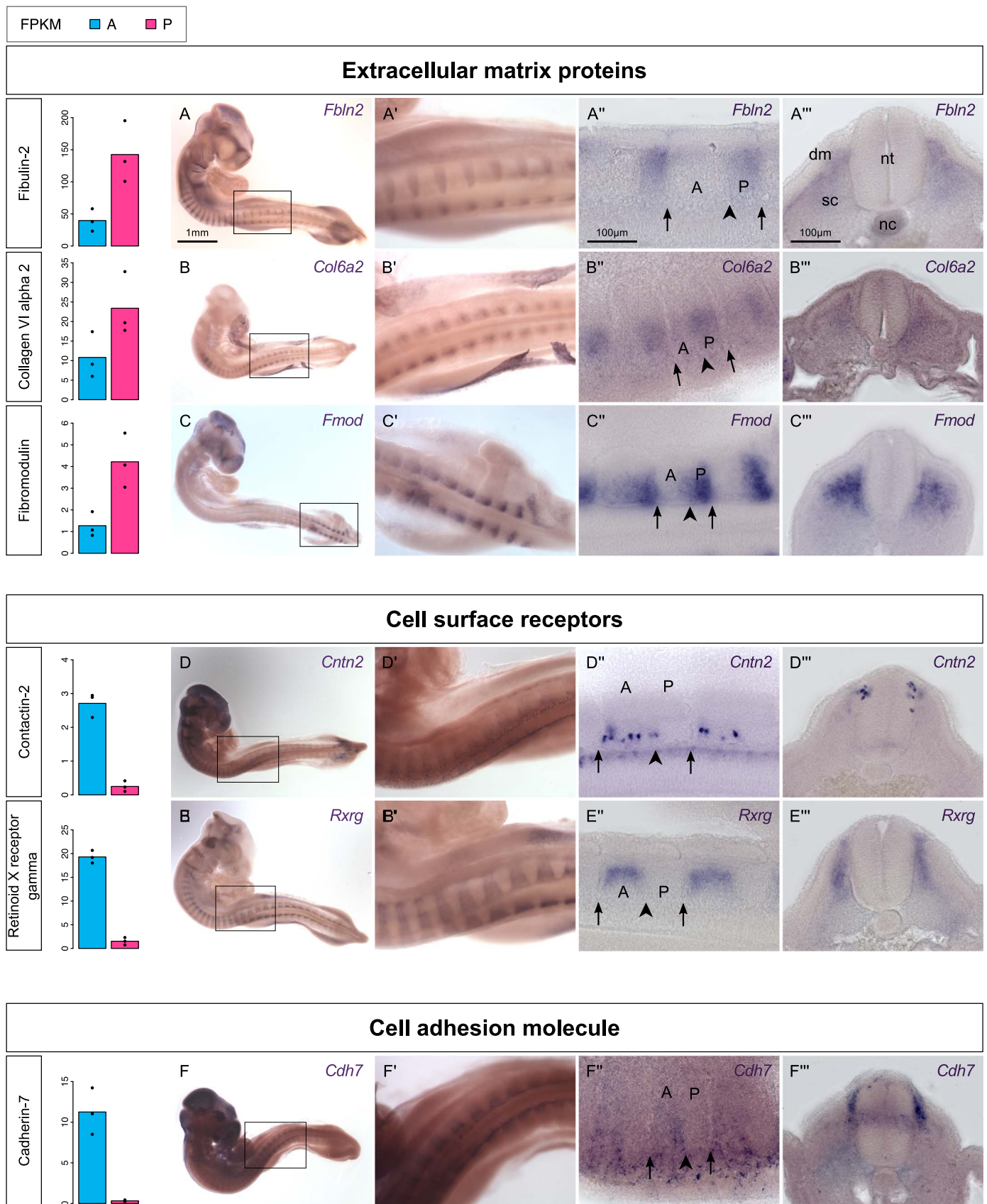


Fig. 3. Validation of genes expressed in anterior or posterior half-sclerotomes by whole-mount *in situ* hybridization. Whole-mount *in situ* hybridization on chick embryos of embryonic day 3 (stage HH18) for the extracellular matrix proteins Fibulin-2 (A), Collagen VI alpha 2 (B) and Fibromodulin (C), expressed in posterior half-sclerotomes; and the cell surface receptors Contactin-2 (D) and Retinoid X receptor gamma (E) and the cell adhesion molecule Cadherin-7 (F), expressed in anterior half-sclerotomes. For each gene, a barplot of FPKM values as determined by RNA-sequencing is given. (A-F) Pictures of whole embryos. (A'-F') Zooms of pictures (A-F). (A''-F'') Representative longitudinal sections. The arrows indicate the intersomitic boundaries between adjacent segments. The arrowhead indicates the intrasegmental boundary between anterior (A) and posterior (P) half-sclerotomes. (A'''-F''') Representative transverse sections. sc: sclerotome. dm: dermomyotome. nt: neural tube. nc: notochord.

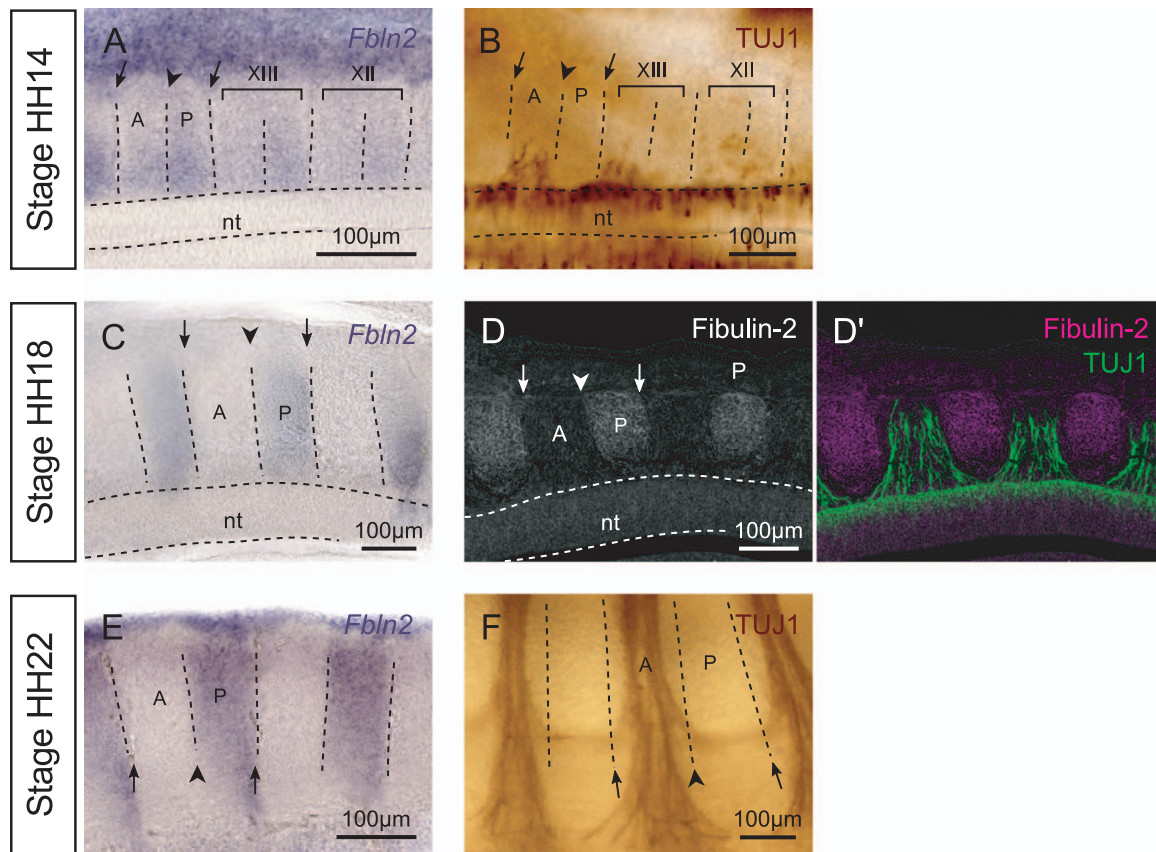


Fig. 4. Fibulin-2 preferential expression in the posterior half-sclerotome coincides with spinal nerve segmental outgrowth. (A) *In situ* hybridization for *Fbln2* on a chick embryo of embryonic day 2.5 (stage HH14). The arrows indicate the intersomitic boundaries between adjacent segments. The arrowhead indicates the intrasegmental boundary between anterior (A) and posterior (P) half-sclerotomes. nt: neural tube. Somite staging is indicated in roman numerals. (B) Tubulin 3 β (TUJ1) whole-mount immunohistochemistry showing spinal neurons in a chick embryo of embryonic day 2.5 (stage HH14). (C) *In situ* hybridization for *Fbln2* on a chick embryo of embryonic day 3 (stage HH18). (D) Fibulin-2 immunohistochemistry on a section of a chick embryo of embryonic day 3 (stage HH18) showing Fibulin-2 expression in the posterior half-sclerotome. (D') Overlay of Fibulin-2 (magenta) and Tubulin 3 β (TUJ1, green). (E) *In situ* hybridization for *Fbln2* on a chick embryo of embryonic day 4 (stage HH22). (F) Tubulin 3 β (TUJ1) whole-mount immunohistochemistry showing spinal neurons in a chick embryo of embryonic day 4 (stage HH22).

repellent Sema3A, which is expressed in the posterior half-sclerotome (Eickholt et al., 1999; Roffers-Agarwal and Gammill, 2009). We used the collapse assay with recombinant proteins to determine if there is a synergy between Fibulin-2 and Sema3A to cause collapse *in vitro*. When pre-incubated together at room temperature for 30 min and after 30 min of treatment, no difference was seen in the percentage of collapsed growth cones for 100 ng/ml Sema3A with and without Fibulin-2 (21.9% versus 24.2%, *t*-test, *P*-value = 0.3846). However, when pre-incubated together at room temperature for 30 min and after 1 h treatment, Fibulin-2 significantly increased the percentage of collapse growth cones in explants treated with 100 ng/ml Sema3A to 34.9%, compared to 24.8% for Sema3A only (*t*-test, *P*-value = 5.81e-04) (Fig. 6B). The repulsive potential of Fibulin-2 and Sema3A together was comparable to that seen using a higher concentration of Sema3A (300 ng/ml) (36.4%) (*t*-test, *P*-value = 0.684). As a control, treatment with Fibulin-2 alone (250 ng/ml) did not show any significant effect after 1 h (16.2% for PBS control versus 18.2% for 250 ng/ml Fibulin-2) (*t*-test, *P*-value = 0.241) (Fig. 6C).

We tested this effect with another cue with repulsive properties expressed in the posterior half-sclerotome, Sema3F. We found no similar effect of Fibulin-2 on the percentage of collapsed growth cones when pre-incubating the recombinant molecules for 30 min and treating the cultures for 1 h (23.8% for 300 ng/ml Sema3F versus 20.7% for 300 ng/ml Sema3F with 250 ng/ml Fibulin-2, *t*-test, *P*-value = 0.381) (Fig. 6D).

Together, these experiments show that Fibulin-2 does not have an intrinsic axon growth repulsive activity, but enhances Sema3A repulsive activity *in vitro*.

2.5. Fibulin-2 is expressed by reactive astrocytes following adult CNS injury

Based on the molecular characterization of anterior and posterior half-sclerotomes in the chick embryo, we have identified the extracellular matrix protein Fibulin-2 as a regulator of spinal nerve organization. The identification of molecular players of axon guidance during development provides valuable information on the potential for axon regeneration in the adult CNS (Giger et al., 2010; Hilton and Bradke, 2017), in particular on the role and structure of the extracellular environment and its impact on axon growth following injury.

Using a mouse model of cerebral cortical stab injury (1 week post-injury), we observed that in the contralateral (control) side Fibulin-2 has a basal, diffuse expression in the brain, while in the injured side Fibulin-2 is detected with a higher intensity at focal points, close to the edge of the lesion (Fig. 7A–D). The staining intensity as measured by the raw integrated density was significantly higher in the injured side compared to the control side (1.5-fold increase, *t*-test, *P*-value = 4.95e-03) (Fig. 7E). Individual Fibulin-2-positive cells with large protrusions could be observed. Co-staining with glial fibrillary acidic protein (GFAP) revealed that these Fibulin-2-positive cells are reactive astrocytes accumulating at the lesion site (Fig. 7F and G and Supplementary material Fig. 5). We also looked at Fibulin-2 expression in a crush model of spinal cord injury in rat (Moendarbary et al., 2017). Immunostaining was carried out on transverse sections of injured spinal cord, 1 week and 3 weeks post-injury. We observed that Fibulin-2 expression is increased in the glial scar region, which acts as a barrier for axon growth, with intense depositions around the cyst cavity

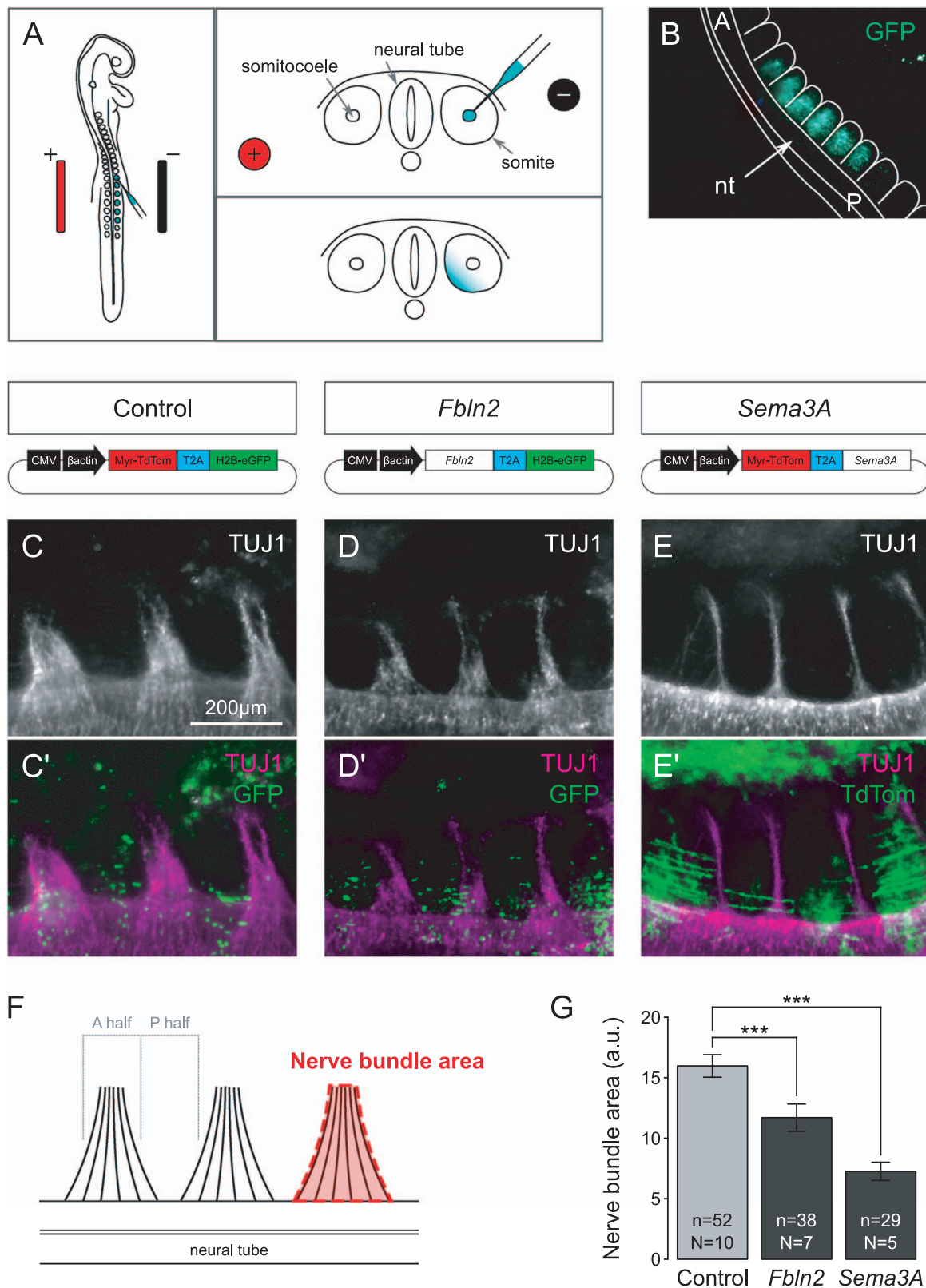


Fig. 5. Fibulin-2 overexpression restricts locally spinal nerve outgrowth. (A) Principle of somite electroporation. Schematic drawing of a chick embryo of stage HH14. (B) Picture of a live chick embryo of stage HH18 24 h post-electroporation, showing expression of the reporter gene GFP in 6 consecutive segments. A: anterior end of the embryo. P: posterior end. nt: neural tube. (C-E) Whole-mount immunohistochemistry for Tubulin 3β (TUJ1) showing spinal nerve outgrowth 24 h after electroporation with control plasmid (Myr-TdTomato/T2A/H2B-GFP), *Fbln2* or *Sema3A* expression vector, respectively. (C'-E') Overlay of Tubulin 3β (TUJ1, magenta) and GFP or TdTomato (green). (F) Schematic representation of quantification method of nerve bundle area. The area of spinal nerve bundle is measured for each bundle in GFP-positive segments. (G) Quantification of the nerve bundle area (arbitrary units, a.u.) in segments electroporated with control plasmid (16.0 ± 0.9), with *Fbln2* expression vector (11.7 ± 1.1) or with *Sema3A* expression vector (7.3 ± 0.7). Data are expressed as mean of the nerve bundle area ± standard error of the mean, with n the number of GFP-positive segments and N the number of embryos. T-test, *** P-value < 0.001.

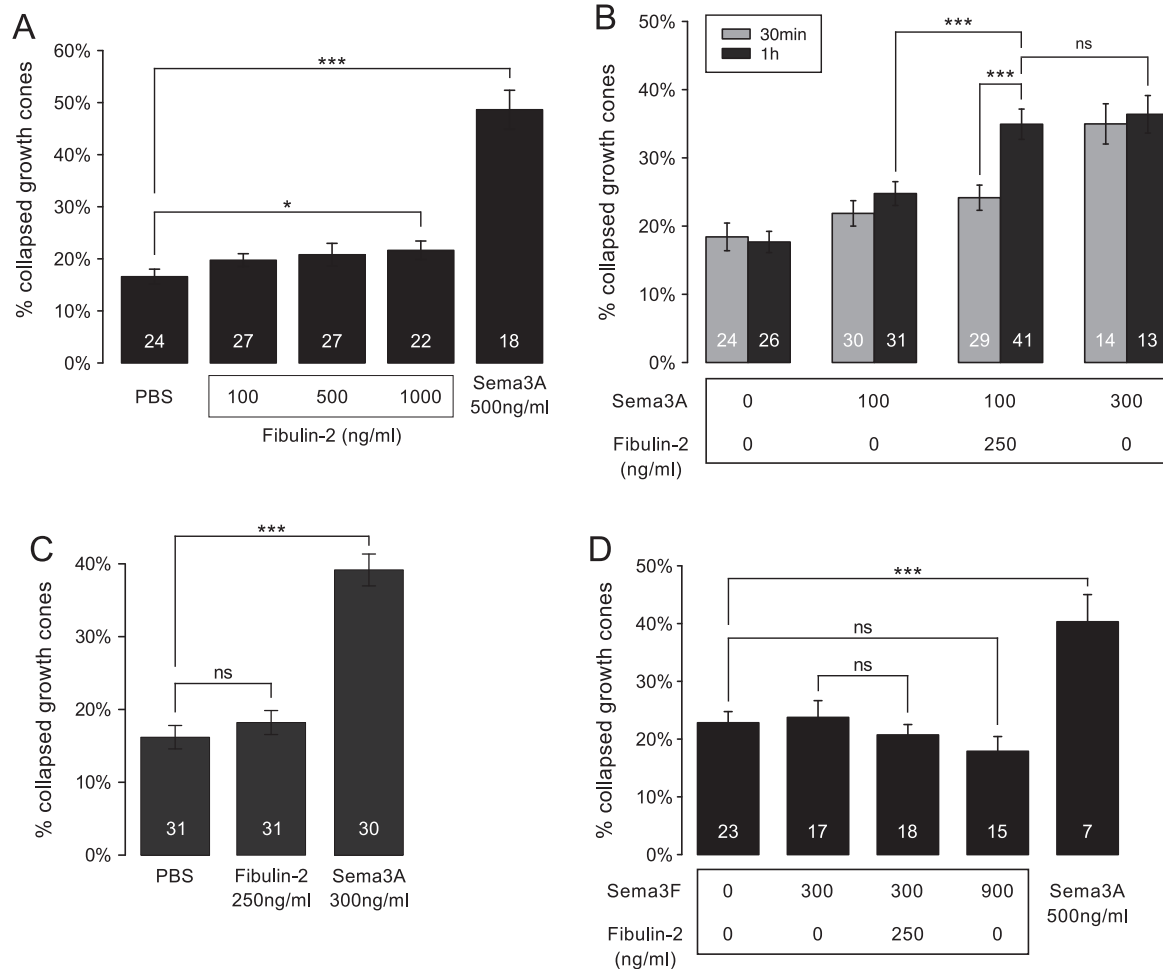


Fig. 6. Fibulin-2 enhances the repulsive activity of the axon growth repellent Sema3A. (A) Growth cone collapse assay testing the repulsive activity of Fibulin-2 at various concentrations on chick dorsal root ganglion (DRG) cultures for 30 min (B) Collapse assay testing the repulsive activity of Sema3A alone versus Sema3A plus Fibulin-2 for 30 min and 1 h. Fibulin-2 and Sema3A were mixed and incubated together for 30 min at room temperature before treatment. (C) Collapse assay testing the repulsive activity of Fibulin-2 alone for 1 h. (D) Collapse assay testing the repulsive activity of Sema3F alone versus Sema3F plus Fibulin-2 for 1 h. Fibulin-2 and Sema3F were mixed and incubated together for 30 min at room temperature before treatment. Recombinant human Sema3A, recombinant human Fibulin-2 and recombinant mouse Sema3F were used. Data are expressed as mean of the percentage of collapsed growth cones ± standard error of the mean, with n the number of DRG explants (indicated at the bottom of each bar). T-test, *P < 0.05, ***P < 0.001, ns: not significant.

(Supplementary material Fig. 6A–C). We quantified this increase by measuring the staining intensity in regions corresponding to the lesion site (Supplementary material Fig. 6D) and we found that Fibulin-2 expression is significantly higher in this region 1 week and 3 weeks post-injury compared to the corresponding region in uninjured animals (2.6- and 2.7-fold increase, *t*-test, *P*-value = 6.62e-03 and 2.04e-04 respectively) (Supplementary material Fig. 6E).

Together, these results show that Fibulin-2 expression increases after CNS injury, specifically in reactive astrocytes accumulating at the lesion.

3. Discussion

The vertebral column is a fundamental structure characteristic of vertebrates that provides robustness and flexibility to the body, while simultaneously protecting the spinal cord. The molecular dissection of its development is crucial to our understanding of vertebrate organization and evolution, and to give insight into extrinsic axon guidance mechanisms with implications for CNS repair and regeneration. In the vertebrate trunk the antero-posterior polarization of each segment allows functional integration of the spinal nerves in the vertebral column. Here, we have investigated the molecular basis of sclerotome antero-posterior subdivision in relation to spinal nerve segmentation using RNA-sequencing. This is the first high-throughput sequencing analysis of this system in the chick embryo, and this has led to the

identification of differentially expressed genes previously uncharacterized in this system, such as the ECM proteins Fibulin-2, Fibromodulin and Collagen VI alpha 2 that are expressed in the posterior half-sclerotome. We found a particular enrichment of ECM and ECM-associated proteins in this system, that may participate in the adhesive or repulsive properties required for spinal nerve outgrowth, in the control of cell segregation between anterior and posterior half-sclerotomes, and in the mechanical properties of sclerotomes.

We focused on Fibulin-2, one ECM glycoprotein potentially involved in the contact-repulsion mechanism of axon growth present in the posterior half-sclerotome. We confirmed that Fibulin-2 is expressed in the posterior half-sclerotome, both at the mRNA and at the protein levels, and we found that the segmented pattern of expression of Fibulin-2 coincides with the initial segmented outgrowth of spinal nerves. Using *in ovo* and *in vitro* approaches, we investigated its potential for axon growth repulsion, and found that it enhances Sema3A repulsive activity to promote growth cone collapse *in vitro*. In addition, the area of spinal nerve bundles was restricted by Fibulin-2 overexpression in sclerotomes, suggesting a role of the extracellular matrix protein Fibulin-2 in controlling the path of outgrowing spinal axons.

3.1. The ECM in the local regulation of axon pathfinding

Our results suggest a role for Fibulin-2 in the spatial distribution of

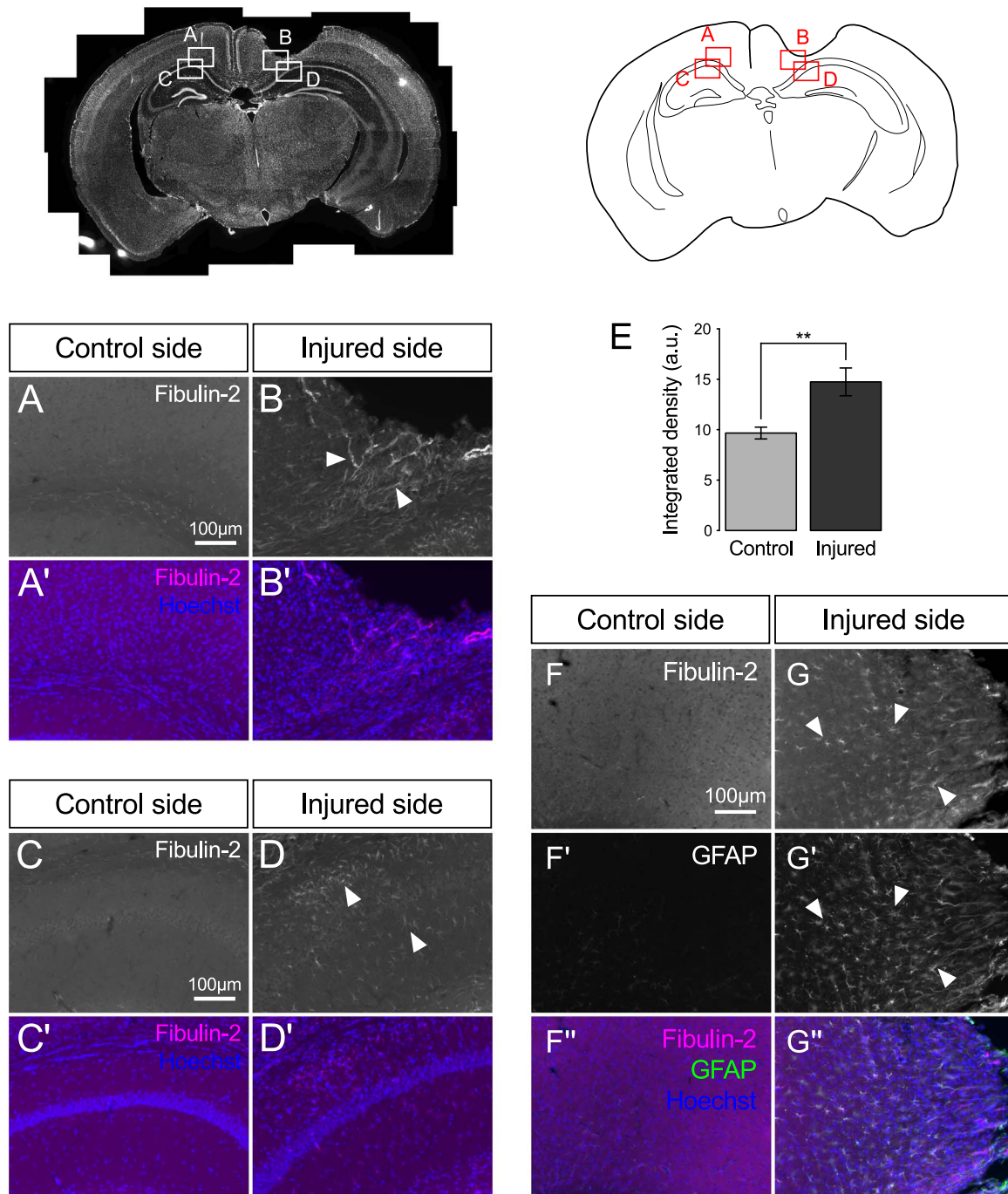


Fig. 7. Fibulin-2 protein expression is increased in astrocytes following traumatic brain injury. Picture of a coronal section of an injured mouse brain (Hoechst staining) and corresponding schematic representation. (A-D) Fibulin-2 immunohistochemistry on a section of an injured mouse brain showing Fibulin-2 expression in the contralateral (control) side (pictures (A) and (C)) and the injured side (pictures (B) and (D)). Arrowheads indicate positive staining. (A'-D') Overlay of Fibulin-2 (magenta) and Hoechst (nuclear staining, blue) corresponding to pictures (A-D), respectively. (E) Barplot representing the staining intensity in control side and in injured side. Data are expressed as mean of the raw integrated density (in arbitrary units, a.u.) \pm standard error of the mean. The quantification is done on $n = 12$ representative pictures of the lesion area and $n = 12$ representative pictures of the corresponding contralateral region over $N = 4$ animals. T-test, $**P < 0.01$. (F-G) Fibulin-2 immunohistochemistry on a section of an injured mouse brain showing Fibulin-2 expression in the contralateral (control) side (F) and the injured side (G). (F'-G') GFAP immunohistochemistry. Arrowheads indicate positive staining. (F''-G'') Overlay of Fibulin-2 (magenta), GFAP (green) and Hoechst (nuclear staining, blue). Pictures are representative of $N = 4$ animals.

axon growth repulsion. Fibulin-2 autonomous repulsive activity was tested *in vitro* using the growth cone collapse assay. While Fibulin-2 by itself did not cause major collapse, Fibulin-2 in combination with Sema3A increased the proportion of collapsed growth cones compared to Sema3A alone. The advantages of this developmental system could be to minimize the amount of diffusible Sema3A required and to potentiate the repulsive activity of Sema3A over time to finely shape nerve trajectories. A similar role has been shown for the neurotrophic

factor GDNF, which does not have axon guidance properties by itself, but which modulates the response of commissural growth cones to Sema3B when they cross the midline (Charoy et al., 2012). Another similar type of sensitization effect has been described in the perineuronal nets (PNNs) of the adult brain to control CNS plasticity (Dick et al., 2013). In this case, the CS-E motif of chondroitin sulfate proteoglycans (CSPGs) synergizes with Sema3A to restrict neurite length *in vitro*. In the developing vertebral column, Fibulin-2 may

present the diffusible repellent cue *Sema3A* to navigating growth cones and enhance its collapse-inducing activity potentially via an interaction with *Nrp1* receptor at their surface, in order to maintain their sensitivity to *Sema3A*. Desensitization to *Semaphorin 3* repellent cues has been observed *in vitro* over time, and its regulation depends on protein synthesis-dependent responses to varying repellent concentrations (Piper et al., 2005), as well as on proteolytic degradation of *Nrp1* receptor (Romi et al., 2014). Here, the functional association of *Fibulin-2* and *Sema3A* may contribute to the maintenance of a robust repulsion and hence of the correct spinal nerve compaction until formation of the cartilage of the vertebral column. Whether *Fibulin-2* is a ligand for the *Neuropilin/Plexin* receptor complex in the transduction of *Sema3A* repulsive signaling (Takahashi et al., 1999) remains to be determined.

In addition to enhancing *Sema3A* repulsive activity, *Fibulin-2* might also act as a scaffold for this type of diffusible repellent, by stabilizing its position in the posterior half-sclerotome and contributing to the tight shaping of the boundaries between nerve and cartilage tissues. Although our *in vitro* data suggest that the potentiation effect of *Fibulin-2* is specific to *Sema3A*, we do not exclude that *Fibulin-2* enhances the repulsive activity of other repellent cues expressed in the posterior half-sclerotome. *Fibulin-2* has been shown to interact with *Versican* (Olin et al., 2001), a CSPG with growth-inhibitory properties that is also expressed in the posterior half-sclerotome (Landolt et al., 1995; Perissinotto et al., 2000). More generally, fibulins interact with a wide range of ECM ligands, including fibronectin, fibrillins, nidogen and proteoglycans (Sasaki et al., 1995; Hopf et al., 1999; Olin et al., 2001; Vega et al., 2009). These interactions are Ca^{2+} -dependent and support their role as scaffolding proteins in matrix-matrix and cell-matrix networks. In the posterior half-sclerotome *Fibulin-2* may provide an impenetrable scaffold for axons to grow adjacent to it, allowing a tight spatiotemporal control of axon pathfinding. It is also possible that overexpression of *Fibulin-2* enhances the fasciculation of spinal nerve bundles, leading to the higher compaction observed in experimental embryos. Misexpressing *Fibulin-2* in the anterior half-sclerotome could create a sink of this ECM anchor that axons use to fasciculate and to form tight bundles.

3.2. Composition of the ECM in the glial scar following adult CNS injury

The elucidation of the molecular regulation of spinal nerve growth during development provides insight into the control of connectivity and plasticity in the adult CNS. In the normal adult CNS, the ECM has specific functions in the regulation of neural activity, of synaptic connectivity and of stem cell niches. Some ECM and guidance molecules secreted during development may have basal or low expression at the adult age, but are upregulated by reactive astrocytes that accumulate at the lesion site and participate in the scarring process of the injured tissue following injury to the CNS (Silver and Miller, 2004; Jones and Bouvier, 2014; Ohtake and Li, 2015). These include members of the *Semaphorin class 3* family and CSPGs such as *Aggrecan*. These astrocyte-induced changes in ECM composition and structure are linked with their role in the scarring process after brain or spinal cord injury.

Here we looked at *Fibulin-2* expression in the adult injured CNS. Our results show an increase of *Fibulin-2* expression in reactive astrocytes at the injury site. *Fibulin-2* has been shown to play a role in cell adhesion and cell migration in various physiological and pathological conditions, e.g. wound healing and cancer progression (Yi et al., 2007; Alcendor et al., 2011; Law et al., 2012; Fontanil et al., 2014). In addition, as a key ECM organizer, *Fibulin-2* could participate in the remodeling of the ECM at the site of the glial scar and in the migratory properties of astrocytes, as well as in the functional reorganization of the circuits. As a binding partner of *Aggrecan* and *Versican* (Olin et al., 2001), it is possible that *Fibulin-2* interacts with

these molecules in specific ECM structures in the CNS, such as PNNs.

We found that proteins expressed in the posterior half-sclerotome (a proto-cartilage structure) are also expressed in the glial scar following traumatic spinal cord injury. This is the case of *Periostin*, the small glycoprotein *Fibromodulin* and *Collagen VI alpha 2* that are enriched in the ECM of injured spinal tissue, as identified in a high-throughput proteomics screen (Didangelos et al., 2016). Various types of collagens and ECM proteins have been found in a molecular characterization of spinal cord injury by RNA-sequencing and are thought to act as a scaffold for cell adhesion during scar formation (Hara et al., 2017). The glial scar also acts as a mechanical and chemical barrier to axon regeneration, and degradation of CSPGs, growth-inhibiting ECM components, is one therapeutic approach that leads to significant motor recovery in rat models of spinal cord injury (García-Álías et al., 2009; James et al., 2015). ECM remodeling underlies multiple events of the scarring process: migration of astrocytes (Hsu et al., 2008), consolidation of the scar (Jones and Bouvier, 2014), limitation of inflammatory events (Faulkner et al., 2004), cell-matrix signaling (Didangelos et al., 2016), and regulation of CNS plasticity following injury (Dick et al., 2013). Therefore, elucidation of the ECM composition and functions is critical for the design of effective CNS repair strategies.

Our study provides an updated molecular characterization of anterior and posterior half-sclerotomes in amniotes. In addition to validating genes previously uncharacterized in this system, our results support a role for the ECM molecule *Fibulin-2* in regulating spinal nerve outgrowth, potentially via a functional interaction with *Sema3A*. This developmental mechanism of axon pathfinding may be reactivated in the adult CNS following traumatic injury, providing insight into the potential for regeneration in adult tissues.

4. Material and methods

4.1. Dissection of half-sclerotomes

Anterior and posterior half-sclerotomes were dissected from chick embryos of embryonic day 3 (stage HH18). The amnion was removed and the head cut. The embryo was pinned at each extremity of the neural tube, with the dorsal part facing up. A somite strip was isolated on one side of the embryo, by cutting it away from the neural tube and cutting the limb buds. Half-sclerotomes from the anterior or the posterior side of each somite were dissected from the 11th most recent (posterior) segment and up to 12 segments anterior to it. For each half-segment, the ectoderm and the dermomyotome were removed. Half-sclerotomes were washed in ice-cold diethyl pyrocarbonate-treated PBS (DEPC-PBS), then pooled by type in Eppendorf tubes and immediately frozen on dry ice. The tissue was kept at -80°C until RNA extraction.

4.2. RNA extraction, library preparation and sequencing

RNA extraction was done using High Pure RNA Isolation kit (Roche) and the concentration determined with NanoDrop ND-1000 Spectrophotometer (Labtech International). cDNA libraries were prepared from about 200 ng total RNA. RNA samples were polyA selected and single-end sequencing libraries were constructed with TruSeq Stranded mRNA HT Sample Prep kit (Illumina). Sequencing was performed at CRUK Cambridge Institute Core Genomics Illumina Sequencing platforms. Sequencing was 50 base single-end. Adapters were trimmed as part of the Illumina sequencing pipeline. For each sample, sequencing quality was visualized with FastQC (<http://www.bioinformatics.babraham.ac.uk/projects/fastqc>). The quality control of the sequencing showed high quality base calls with an average Phred score > 28 for all samples, so no filtering was performed for the rest of the analysis. Single-end sequence reads were aligned to Galgal4 chicken reference genome (*Gallus gallus*-4.0 (GCA_000002315.2) downloaded from Ensembl (Aken et al., 2017)) using Tophat2 aligner

(version 2.1.0) (Kim et al., 2013). Identification of differentially expressed genes was performed using Cuffdiff (Cufflinks version 2.2.1) (Trapnell et al., 2013). In Supplementary material Table 2, the log₂ fold change was used to improve the symmetry of the data distribution around 0. On the log₂ scale, 1 unit (+1 or -1) represents a 2-fold change between the samples. Data were visualized with the R package CummeRbund (Goff et al., 2013). RNA-sequencing data are deposited in the NCBI Gene Expression Omnibus (GEO) database under accession code GSE103748.

4.3. Functional annotation and clustering visualization

Functional classification of genes differentially expressed was performed with DAVID Bioinformatics Resources 6.8 (Dennis et al., 2003). Functional clustering was visualized with the plug-in Enrichment Map (Merico et al., 2010) from Cytoscape (version 3.6.0) (Shannon et al., 2003).

4.4. Whole-mount *in situ* hybridization

Chick embryos of embryonic day 3 (stage HH18) were fixed in 4% formaldehyde in PBS overnight at 4 °C. Embryos were dehydrated in methanol and kept at -20 °C until required. Whole-mount *in situ* hybridization was performed as described in (Modrell et al., 2011). For template preparation, genes of interest were amplified by PCR using gene-specific primers from chick somite cDNA (Supplementary material Table 3) and cloned into pDrive cloning vector (PCR cloning kit, Qiagen). Antisense RNA probes were synthesized using T7 or SP6 polymerases (Promega) and digoxigenin-labeled dUTPs (Roche). Embryos were graded through 25%, 50% and 70% glycerol in PBS prior to imaging. Embryos were laid in a drop of glycerol in a small Petri dish and imaged with a Leica MZ FL III stereomicroscope. After whole-mount *in situ* hybridization, embryos were embedded in 15% gelatin. Blocks were fixed in 4% formaldehyde overnight at 4 °C before vibratome sectioning (45 µm thick sections). Sections were imaged with a Zeiss Axio Scan.Z1 slide scanner.

4.5. Whole-mount immunohistochemistry

Chick embryos of embryonic day 3 (stage HH18) were fixed in 4% formaldehyde in PBS overnight at 4 °C. Embryos were dehydrated in methanol and kept at -20 °C until required. Embryos were rehydrated in PBS 0.1% Triton X-100. Embryos were blocked in PBS 0.5% Triton X-100 (PBS-T) 10% goat serum for at least 3 h at room temperature. Embryos were incubated in primary antibody (mouse anti-Tubulin 3β (TUJ1), BioLegend, cat. n. 801202, and mouse anti-GFP, Roche, cat. n. 11814460001) 1:250 in blocking solution overnight at 4 °C. Embryos were incubated with Alexa Fluor[®]-labeled secondary antibodies (ThermoFisher Scientific) or HRP-labeled secondary antibody (Jackson ImmunoResearch) in blocking solution overnight at 4 °C. For HRP staining, embryos were incubated with 500 µg/ml DAB substrate and 0.006% H₂O₂ in PBS 0.5% Triton. The colour reaction was developed for 5–15 min at room temperature. Embryos were flat-mounted with Fluoromount-G (SouthernBiotech) and imaged with fluorescence microscopy (Zeiss Axioplan 2).

4.6. Immunohistochemistry

Chick embryos of embryonic day 3 (stage HH18) were fixed in 4% formaldehyde overnight at 4 °C and embedded for wax sectioning (6–10 µm thick sections). For anti-Fibulin-2 immunostaining, sections were subjected to heat-induced epitope retrieval (90 °C for 10 min in citrate buffer (10 mM trisodium citrate, HCl to pH 6.0)). Sections were blocked with PBS 5% goat serum for 1 h at room temperature. Sections were incubated with primary antibodies overnight at 4 °C or at room temperature. Primary antibodies used were: rabbit anti-Fibulin-2

(Sigma, cat. n. HPA001934), 1:100; mouse anti-GFP (Roche, cat. n. 11814460001), 1:250; rabbit anti-RFP (Rockland, cat. n. 600-401-379), 1:250; mouse anti-Tubulin 3β (TUJ1) (BioLegend, cat. n. 801202), 1:250; chicken anti-GFAP (Abcam, cat. n. ab4674), 1:1000. Sections were incubated with Alexa Fluor[®]-labeled secondary antibodies (ThermoFisher Scientific) for 2 h at room temperature. Nuclear staining was performed with Hoechst (Roche) diluted 1:5000 in PBS. Slides were mounted with Fluoromount-G (SouthernBiotech). Sections were observed with fluorescence microscopy (Zeiss Axioplan 2).

4.7. Cloning

Full-length chick Fibulin-2 and full-length chick *Sema3A* were amplified from chick somite cDNA with Q5[®] High-Fidelity DNA Polymerase (New England Biolabs). Full-length chick Fibulin-2 with the 60-nucleotide T2A sequence fused at the 3' end was cloned into pT2AL-CMV/βactin-Tomato-T2A-GFP expression vector (Bourgeois et al., 2015), downstream of CMV/βactin, and upstream of and in frame with the reporter H2B-eGFP. The primer sequences to amplify chick Fibulin-2 were: 5'-GGGAAGACTATGGATAGGCACCA-3' (forward) and 5'-GTATGTATGAGCTGTGATGAAAATG-3' (reverse). Full-length chick *Sema3A* was cloned into pT2AL-CMV/βactin-Tomato-T2A-GFP expression vector, downstream of CMV/βactin and Myr-TdTomato. The primer sequences to amplify chick *Sema3A* were: 5'-TCGCAGGGACCC TACAGTG-3' (forward) and 5'-TGAGGTTTCTAGAGGTAATGTAGC-3' (reverse). The original pT2AL-CMV/βactin-Tomato-T2A-GFP expression vector was used as the control plasmid.

4.8. Somite electroporation

Somite electroporation was performed as described in (Wang et al., 2011), with the only difference that the medio-ventral region of somites (presumptive sclerotome) was targeted. Chick embryos of stage HH13–14 (18–22 somites) were prepared for electroporation. Electrodes (2 mm in length) were positioned on each side of the embryo, above the vitelline vessels. Four to six somites of the right-hand side of the neural tube were targeted. The plasmid solution, containing 1.4–1.8 µg/µl expression vector and 5% FastGreen, was injected by mouth pipetting into the somitocoele, using borosilicate glass capillaries (outside diameter 1 mm, inside diameter 0.58 mm) (World Precision Instruments) that were drawn on a needle puller PC-10 (Narishige) at 62 °C. Current was applied using an ECM 830 Square Wave Pulse generator (BTX Instrument Division, Harvard Apparatus, Inc.) with the following settings: 50 V, 5 pulses of 20 ms, with 500 ms interpulse interval. The egg was sealed with Parafilm M[®] and placed in a humidified incubator at 37.5 °C. Embryos were observed after 24 h with a Leica MZ FL III fluorescence stereomicroscope to control for the survival and stage of development, as well as the expression of the reporter gene in targeted segments. Embryos of stage HH18 were kept for the analysis. Embryos that had major electroporation-related trunk malformations or that had a low GFP expression were discarded for the analysis. Spinal nerve bundle area was quantified for each GFP-positive segment at the same axial level in electroporated embryos. Area measurements were done with ImageJ (Schindelin et al., 2012).

4.9. Growth cone collapse assay

Collapse assays were performed according to (Kapfhammer et al., 2007). Coverslips were coated with poly-L-lysine (0.01%) (Sigma) and 40 µg/ml laminin (Sigma). Dorsal root ganglia (DRG) were dissected from chick embryos of embryonic day 7, and cultured in DRG culture medium (DMEM supplemented with insulin-transferrin-sodium selenite (ITS) supplement (Sigma), penicillin-streptomycin glutamine (Sigma) and 5 ng/ml nerve growth factor (NGF) (Sigma)). DRG explants were treated after 24 h culture. Treatments were blind-coded and randomly assigned to each culture to minimize scoring bias.

Recombinant human Sema3A (R & D Systems), recombinant human Fibulin-2 (Novus Biologicals) and recombinant mouse Sema3F (R & D Systems) were used in collapse assays. Neuronal cultures were incubated at 37 °C and 5% CO₂ for 30 min to 1 h, then fixed with 4% formaldehyde and 15% sucrose in PBS, pH 7.4. Axons were observed with phase-contrast microscopy (Zeiss Axiovert 25). 30–50 axons per explant were scored, which corresponds to axons that grew the furthest away from the explant and isolated enough from their neighbours. Each growth cone was scored as spread (flattened lamellipodia, more than 3 filopodia) or collapsed (needle-shaped tip, less than 2 filopodia). Each growth cone collapse assay was repeated three independent times.

4.10. Mouse cortical stab injury

All animal work was carried out in accordance with national law and regulation in accordance with the UK Animals Scientific Procedures Act (1986). Animals used in this study were housed in standard housing conditions with a 12 h light/dark cycle. Where possible, animals were housed in groups of 2–5 per cage. Animals were fed and watered *ad libitum*. C57BL6 mice received a right hemisphere cortical stab wound injury. Surgery was conducted stereotactically under isoflurane (2–3%, 0.2 L/min) anaesthesia. Briefly, a section of the skull was removed and cortical tissue was exposed. A single 1 mm deep stab wound injury was created by inserting and drawing a microscalpel blade from bregma \approx from antero-posterior: -2, ventral: -1.0, lateral: 3.0 to antero-posterior: -4, ventral: -1.0, lateral: 3.0. Skull was resealed using sterile beeswax and mice were allowed to recover in a heated chamber. For post-operative pain management, animals received oral doses of Meloxicam (Metacam, 0.1 ml / 10 g). Seven days following surgery animals were sacrificed and transcardially perfused with 4% formaldehyde (100 ml total volume). Tissue was removed and placed in formaldehyde for an additional 24 h, after which it was transferred to 30% sucrose in PBS for cryoprotection. For immunohistochemical analysis 30 μ m thick sections were cut on a freezing microtome and stained as described in paragraph Immunohistochemistry. For image analysis, the background was subtracted with ImageJ (Schindelin et al., 2012) (rolling ball radius: 50 pixels) prior to measurement of raw integrated density.

4.11. Rat spinal cord injury

Sections of normal and injured rat spinal cord were kindly provided by Dr Isabel Weber, Franze research group, Department of Physiology, Development and Neuroscience, and Dr Barbara Haenzi, Fawcett research group, John van Geest Centre for Brain Repair, Cambridge. Animals underwent spinal cord dorsal column crush injury as described in (Moeendarbary et al., 2017). Spinal cords were fixed at about one week and three weeks post-injury and sectioned with a cryostat. Sections (14 μ m thick) were immunostained as described in paragraph Immunohistochemistry. For image analysis, the background was subtracted with ImageJ (Schindelin et al., 2012) (rolling ball radius: 50 pixels) prior to measurement of raw integrated density.

4.12. Quantification and statistical analysis

Power calculations and statistical analysis were performed with R (R Core Team, 2014). For each condition, the Shapiro-Wilk test for normality was used to assess normal distribution of data (P -value \geq 0.01). Datasets that were not normally distributed were subjected to a log₁₀ transformation before statistical analysis. P -values were calculated with two-tailed t -test to compare two conditions.

Acknowledgements

We thank Dr Delphine Duprez and Dr Claire Fournier-Thibault

(Institut de Biologie Paris Seine, France) for kindly providing the pT2AL-CMV/ β actin-Tomato-T2A-GFP plasmid. We thank Dr Barbara Haenzi (John van Geest Centre for Brain Repair, Cambridge, UK) and Dr Isabel Weber (Department of Physiology, Development and Neuroscience, University of Cambridge, UK) for kindly providing the rat spinal cord sections. We thank Prof. Magdalena Zernicka-Goetz for providing the anti-RFP antibody. We thank Prof. William Harris for critical reading of the manuscript; Prof. Christine Holt, Dr Clare Baker and Dr Kristian Franze for helpful discussions as well as for sharing of reagents; and Dr Angeleen Fleming, Dr Homaira Nawabi and Dr Stéphane Belin for helpful comments. We thank Béatrice Blot, the Nawabi research group and the Photonic and Imaging Centre at Grenoble Institute of Neuroscience (Grenoble, France) for their kind help in completing this manuscript. The Photonic Imaging Center of Grenoble Institute Neuroscience (Univ Grenoble Alpes – Inserm U1216) is part of the ISdV core facility and certified by the IBISA label.

This project was supported by the International Spinal Research Trust (registered charity) (Nathalie Rose Barr Studentship, ref. RG71958) and the Rosetrees Trust (ref. M317).

Appendix A. Supplementary material

Supplementary data associated with this article can be found in the online version at doi:10.1016/j.ydbio.2018.06.014.

References

- Aken, B.L., Achuthan, P., Akanni, W., Amode, M.R., Bernsdorff, F., Bhai, J., Billis, K., Carvalho-Silva, D., Cummins, C., Clapham, P., et al., 2017. Ensembl 2017. *Nucleic Acids Res.* 45, D635–D642.
- Alcendor, D.J., Knobel, S., Desai, P., Zhu, W.Q., Hayward, G.S., 2011. KSHV regulation of Fibulin-2 in Kaposi's sarcoma: implications for tumorigenesis. *Am. J. Pathol.* 179, 1443–1454.
- Bai, G., Chivatakarn, O., Bonanomi, D., Lettieri, K., Franco, L., Xia, C., Stein, E., Ma, L., Lewcock, J.W., Pfaff, S.L., 2011. Presenilin-dependent receptor processing is required for axon guidance. *Cell* 144, 106–118.
- Bonanomi, D., Pfaff, S.L., 2010. Motor axon pathfinding. *Cold Spring Harb. Perspect. Biol.* 2, a001735.
- Bourgeois, A., Esteves de Lima, J., Charvet, B., Kawakami, K., Stricker, S., Duprez, D., 2015. Stable and bicistronic expression of two genes in somite- and lateral plate-derived tissues to study chick limb development. *BMC Dev. Biol.* 15, 39.
- Bronner-Fraser, M., Stern, C., 1991. Effects of mesodermal tissues on avian neural crest cell migration. *Dev. Biol.* 143, 213–217.
- Charoy, C., Nawabi, H., Reynaud, F., Derrington, E., Bozon, M., Wright, K., Falk, J., Helmbacher, F., Kindbeiter, K., Castellani, V., 2012. gdnf activates midline repulsion by Semaphorin3B via NCAM during commissural axon guidance. *Neuron* 75, 1051–1066.
- Christ, B., Ordahl, C.P., 1995. Early stages of chick somite development. *Anat. Embryol. (Berl.)* 191, 381–396.
- Clagett-Dame, M., McNeill, E.M., Muley, P.D., 2006. Role of all-trans retinoic acid in neurite outgrowth and axonal elongation. *J. Neurobiol.* 66, 739–756.
- Dennis, G., Sherman, B.T., Hosack, D.A., Yang, J., Gao, W., Lane, H.C., Lempicki, R.A., 2003. DAVID: database for annotation, visualization, and integrated discovery. *Genome Biol.* 4, P3.
- Dick, G., Tan, C.L., Alves, J.N., Ehlert, E.M.E., Miller, G.M., Hsieh-Wilson, L.C., Sugahara, K., Oosterhof, A., Kuppevelt, T.H., van Verhaagen, J., et al., 2013. Semaphorin 3A binds to the perineuronal nets via chondroitin sulfate Type E motifs in rodent brains. *J. Biol. Chem.* 288, 27384–27395.
- Didangelos, A., Puglia, M., Iberl, M., Sanchez-Bellot, C., Roschitzki, B., Bradbury, E.J., 2016. High-throughput proteomics reveal alarmins as amplifiers of tissue pathology and inflammation after spinal cord injury. *Sci. Rep.* 6, 21607.
- Eickholt, B.J., Mackenzie, S.L., Graham, A., Walsh, F.S., Doherty, P., 1999. Evidence for collapsin-1 functioning in the control of neural crest migration in both trunk and hindbrain regions. *Development* 126, 2181–2189.
- Faulkner, J.R., Herrmann, J.E., Woo, M.J., Tansey, K.E., Doan, N.B., Sofroniew, M.V., 2004. Reactive astrocytes protect tissue and preserve function after spinal cord injury. *J. Neurosci.* 24, 2143–2155.
- Fleming, A., Kishida, M.G., Kimmel, C.B., Keynes, R.J., 2015. Building the backbone: the development and evolution of vertebral patterning. *Development* 142, 1733–1744.
- Fontanil, T., Rúa, S., Llamazares, M., Moncada-Pazos, A., Quirós, P.M., García-Suárez, O., Vega, J.A., Sasaki, T., Mohamedi, Y., Esteban, M.M., et al., 2014. Interaction between the ADAMTS-12 metalloprotease and fibulin-2 induces tumor-suppressive effects in breast cancer cells. *Oncotarget* 5, 1253–1264.
- Fredette, B.J., Miller, J., Ranscht, B., 1996. Inhibition of motor axon growth by T-cadherin substrata. *Dev. Camb. Engl.* 122, 3163–3171.
- García-Alfás, G., Barkhuysen, S., Buckle, M., Fawcett, J.W., 2009. Chondroitinase ABC treatment opens a window of opportunity for task-specific rehabilitation. *Nat.*

- Neurosci. 12, 1145–1151.
- Giger, R.J., Hollis, E.R., Tuszyński, M.H., 2010. Guidance molecules in axon regeneration. *Cold Spring Harb. Perspect. Biol.* 2.
- Goff, L., Trapnell, C., Kelley, D., 2013. *cummeRbund: Analysis, Exploration, Manipulation, and Visualization of Cufflinks High-Throughput Sequencing Data. Version 2.18.0* from Bioconductor.
- Hamburger, V., Hamilton, H.L., 1951. A series of normal stages in the development of the chick embryo. *J. Morphol.* 88, 49–926.
- Hara, M., Kobayakawa, K., Ohkawa, Y., Kumamaru, H., Yokota, K., Saito, T., Kijima, K., Yoshizaki, S., Harimaya, K., Nakashima, Y., et al., 2017. Interaction of reactive astrocytes with type I collagen induces astrocytic scar formation through the integrin-N-cadherin pathway after spinal cord injury. *Nat. Med.* 23, 818–828.
- Hilton, B.J., Bradke, F., 2017. Can injured adult CNS axons regenerate by recapitulating development? *Development* 144, 3417–3429.
- Hopf, M., Göhring, W., Kohfeldt, E., Yamada, Y., Timpl, R., 1999. Recombinant domain IV of perlecan binds to nidogens, laminin–nidogen complex, fibronectin, fibulin-2 and heparin. *Eur. J. Biochem.* 259, 917–926.
- Hsu, J.-Y.C., Bourguignon, L.Y.W., Adams, C.M., Peyrollier, K., Zhang, H., Fandel, T., Cun, C.L., Werb, Z., Noble-Haeusslein, L.J., 2008. Matrix metalloproteinase-9 facilitates glial scar formation in the injured spinal cord. *J. Neurosci.* 28, 13467–13477.
- Huber, A.B., Kania, A., Tran, T.S., Gu, C., De Marco Garcia, N., Lieberam, I., Johnson, D., Jessell, T.M., Ginty, D.D., Kolodkin, A.L., 2005. Distinct roles for secreted semaphorin signaling in spinal motor axon guidance. *Neuron* 48, 949–964.
- James, N.D., Shea, J., Muir, E.M., Verhaagen, J., Schneider, B.L., Bradbury, E.J., 2015. Chondroitinase gene therapy improves upper limb function following cervical contusion injury. *Exp. Neurol.* 271, 131–135.
- Jones, E.V., Bouvier, D.S., 2014. Astrocyte-secreted matricellular proteins in CNS remodelling during development and disease. *Neural Plast.* 2014, e321209.
- Kapfhammer, J.P., Xu, H., Raper, J.A., 2007. The detection and quantification of growth cone collapsing activities. *Nat. Protoc.* 2, 2005–2011.
- Keynes, R., Tannahill, D., Morgenstern, D.A., Johnson, A.R., Cook, G.M., Pini, A., 1997. Surround repulsion of spinal sensory axons in higher vertebrate embryos. *Neuron* 18, 889–897.
- Keynes, R.J., Stern, C.D., 1984. Segmentation in the vertebrate nervous system. *Nature* 310, 786–789.
- Kim, D., Perteza, G., Trapnell, C., Pimentel, H., Kelley, R., Salzberg, S.L., 2013. TopHat2: accurate alignment of transcriptomes in the presence of insertions, deletions and gene fusions. *Genome Biol.* 14, R36.
- Kraus, F., Haenig, B., Kispert, A., 2001. Cloning and expression analysis of the mouse T-box gene *Tbx18*. *Mech. Dev.* 100, 83–86.
- Kuan, C.-Y.K., Tannahill, D., Cook, G.M.W., Keynes, R.J., 2004. Somite polarity and segmental patterning of the peripheral nervous system. *Mech. Dev.* 121, 1055–1068.
- Landolt, R.M., Vaughan, L., Winterhalter, K.H., Zimmermann, D.R., 1995. Versican is selectively expressed in embryonic tissues that act as barriers to neural crest cell migration and axon outgrowth. *Dev. Camb. Engl.* 121, 2303–2312.
- Law, E.W.L., Cheung, A.K.L., Kashuba, V.I., Pavlova, T.V., Zabarovsky, E.R., Lung, H.L., Cheng, Y., Chua, D., Lai-wan Kwong, D., Tsao, S.W., et al., 2012. Anti-angiogenic and tumor-suppressive roles of candidate tumor-suppressor gene, *Fibulin-2*, in nasopharyngeal carcinoma. *Oncogene* 31, 728–738.
- Lewcock, J.W., Genoud, N., Lettieri, K., Pfaff, S.L., 2007. The ubiquitin ligase *Phr1* regulates axon outgrowth through modulation of microtubule dynamics. *Neuron* 56, 604–620.
- Mansouri, A., Yokota, Y., Wehr, R., Copeland, N.G., Jenkins, N.A., Gruss, P., 1997. Paired-related murine homeobox gene expressed in the developing sclerotome, kidney, and nervous system. *Dev. Dyn. Off. Publ. Am. Assoc. Anat.* 210, 53–65.
- Merico, D., Isserlin, R., Stueker, O., Emili, A., Bader, G.D., 2010. Enrichment map: a network-based method for gene-set enrichment visualization and interpretation. *PLoS One* 5, e13984.
- Modrell, M.S., Bemis, W.E., Northcutt, R.G., Davis, M.C., Baker, C.V.H., 2011. Electrosensory ampullary organs are lateral line placode-derived in bony fishes. *Nat. Commun.* 2, 496.
- Moeendarbary, E., Weber, I.P., Sheridan, G.K., Koser, D.E., Soleman, S., Haenzi, B., Bradbury, E.J., Fawcett, J., Franze, K., 2017. The soft mechanical signature of glial scars in the central nervous system. *Nat. Commun.* 8, (ncomms14787).
- Moret, F., Renaudot, C., Bozon, M., Castellani, V., 2007. Semaphorin and neuropilin co-expression in motoneurons sets axon sensitivity to environmental semaphorin sources during motor axon pathfinding. *Development* 134, 4491–4501.
- Ohtake, Y., Li, S., 2015. Molecular mechanisms of scar-sourced axon growth inhibitors. *Brain Res.* 1619, 22–35.
- Olin, A.I., Mörgelin, M., Sasaki, T., Timpl, R., Heinegård, D., Aspberg, A., 2001. The proteoglycans aggrecan and versican form networks with Fibulin-2 through their lectin domain binding. *J. Biol. Chem.* 276, 1253–1261.
- Perissinotto, D., Iacopetti, P., Bellina, I., Doliana, R., Colombatti, A., Pettway, Z., Bronner-Fraser, M., Shinomura, T., Kimata, K., Mørgelin, M., et al., 2000. Avian neural crest cell migration is diversely regulated by the two major hyaluronan-binding proteoglycans PG-M/versican and aggrecan. *Development* 127, 2823–2842.
- Piper, M., Salih, S., Weigl, C., Holt, C.E., Harris, W.A., 2005. Endocytosis-dependent desensitization and protein synthesis-dependent resensitization in retinal growth cone adaptation. *Nat. Neurosci.* 8, 179–186.
- R Core Team, 2014. *R: A Language and Environment for Statistical Computing. R Foundation for Statistical Computing; Vienna, Austria, 2014.*
- Roffers-Agarwal, J., Gammill, L.S., 2009. Neuropilin receptors guide distinct phases of sensory and motor neuronal segmentation. *Development* 136, 1879–1888.
- Romi, E., Gokhman, I., Wong, E., Antonovsky, N., Ludwig, A., Sagi, I., Saftig, P., Tessier-Lavigne, M., Yaron, A., 2014. ADAM metalloproteases promote a developmental switch in responsiveness to the axonal repellent *Sema3A*. *Nat. Commun.* 5, (ncomms5058).
- Sasaki, T., Göhring, W., Pan, T.-C., Chu, M.-L., Timpl, R., 1995. Binding of mouse and human *Fibulin-2* to extracellular matrix ligands. *J. Mol. Biol.* 254, 892–899.
- Scaal, M., 2016. Early development of the vertebral column. *Semin. Cell Dev. Biol.* 49, 83–91.
- Schindelin, J., Arganda-Carreras, I., Frise, E., Kaynig, V., Longair, M., Pietzsch, T., Preibisch, S., Rueden, C., Saalfeld, S., Schmid, B., et al., 2012. Fiji: an open-source platform for biological-image analysis. *Nat. Methods* 9, 676–682.
- Shannon, P., Markiel, A., Ozier, O., Baliga, N.S., Wang, J.T., Ramage, D., Amin, N., Schwikowski, B., Ideker, T., 2003. Cytoscape: a software environment for integrated models of biomolecular interaction networks. *Genome Res.* 13, 2498–2504.
- Silver, J., Miller, J.H., 2004. Regeneration beyond the glial scar. *Nat. Rev. Neurosci.* 5, 146–156.
- Takahashi, T., Fournier, A., Nakamura, F., Wang, L.-H., Murakami, Y., Kalb, R.G., Fujisawa, H., Strittmatter, S.M., 1999. Plexin-neuropilin-1 complexes form functional semaphorin-3A receptors. *Cell* 99, 59–69.
- Trapnell, C., Hendrickson, D.G., Sauvageau, M., Goff, L., Rinn, J.L., Pachter, L., 2013. Differential analysis of gene regulation at transcript resolution with RNA-seq. *Nat. Biotechnol.* 31, 46–53.
- Tucker, R.P., 2001. Abnormal neural crest cell migration after the in vivo knockdown of tenascin-C expression with morpholino antisense oligonucleotides. *Dev. Dyn. Off. Publ. Am. Assoc. Anat.* 222, 115–119.
- Vega, S., de Iwamoto, T., Yamada, Y., 2009. Fibulins: multiple roles in matrix structures and tissue functions. *Cell. Mol. Life Sci.* 66, 1890–1902.
- Wang, H., Bonnet, A., Delfini, M.C., Kawakami, K., Takahashi, Y., Duprez, D., 2011. Stable, conditional, and muscle-fiber-specific expression of electroporated transgenes in chick limb muscle cells. *Dev. Dyn. Off. Publ. Am. Assoc. Anat.* 240, 1223–1232.
- Warrier, S., Nuwayhid, S., Sabatino, J.A., Sugrue, K.F., Zohn, I.E., 2017. *Supt20* is required for development of the axial skeleton. *Dev. Biol.* 421, 245–257.
- Yi, C.-H., Smith, D.J., West, W.W., Hollingsworth, M.A., 2007. Loss of *Fibulin-2* expression is associated with breast cancer progression. *Am. J. Pathol.* 170, 1535–1545.